International Journal of Applied Pharmaceutics

ISSN- 0975-7058 Vol 15, Issue 4, 2023

Original Article

QBD APPROACH FOR THE DEVELOPMENT OF CAPSAICIN-LOADED STEARIC ACID-GRAFTED CHITOSAN POLYMERIC MICELLES

MAYURI KONDA, SUNITHA SAMPATHI*

[1]Department of Pharmaceutics, Gitam School of Pharmacy, GITAM Deemed to be University, Hyderabad, Telangana–502329, India
*Corresponding author: Sunitha Sampathi; *Email: ssampath@gitam.edu

Received: 16 Apr 2023, Revised and Accepted: 19 May 2023

ABSTRACT

Objective: Capsaicin (CAP) is a naturally occurring alkaloid forecasted in the treatment of Alcoholic Hepatitis (AH), but least studied due to its hydrophobicity and low bioavailability. Hence, the present study aimed to optimize the parameters for the synthesis of stearic acid grafted chitosan (CS-g-SA) copolymer and preparation of CAP-loaded CS-g-SA micelles.

Methods: Quality by design (QbD) approach in coordination with "Central composite designs (CCD) and Box–Behnken designs (BBD)" was used to optimize the process parameters.

Results: CS-g-SA was synthesized at 80 °C, 480 min, and 946 rpm, at these optimized conditions, the average particle size and practical yield were found to be 134.70 nm and 85.69%, respectively. Proton Nuclear Magnetic Resonance (^{1}H NMR) spectra depicted a sharp signal at d=1.0 ppm endorsing to -CH_2 group of SA and confirming the formation of CS-g-SA copolymer. Critical micellar concentration (CMC) and amino groups substitute degree (SD %) were found to be 30.3±1.51µg/ml and 21.3±0.58%, respectively. The distinguished peaks of CAP (0.9 and 1.31 ppm) in ^{1}H NMR spectra disappeared, indicating drug loading in the micellar core. Micelles had an average particle size of 163.15 nm and an encapsulation efficiency of 68.45%. The CAP-CS-g-SA was found to be biocompatible in accordance with the hemolysis test. The *in vitro* release pattern showed 86.78 % in 24 h, indicating the slower release of CAP from micelle, whereas 99.48% CAP was released from non-micellar formulations in 6 h.

Conclusion: CAP-CS-g-SA micelle is a promising approach to improve the bioavailability and controlled release of extremely hydrophobic CAP and further *in vivo* studies would be evident for the treatment of AH using CAP-CS-g-SA.

Keywords: Capsaicin, Chitosan, Stearic acid, Micelles, Bioavailability

DOI: https://dx.doi.org/10.22159/ijap.2023v15i4.48101. Journal homepage: https://innovareacademics.in/journals/index.php/ijap

INTRODUCTION

High alcohol intake is a significant risk factor counting many unfavorable health reactions such as Alcoholic Hepatitis (AH), causing morbidity and death [1].

Nearly one million cases of disability-adjusted life years (Daly) were reported in 2016 due to AH. Per head, alcohol utilization has inclined to 6.4 liters (2016) from 5.5 liters (2000). AH accounts for 34.3% of the patient population in India who suffer from liver-related diseases (2010). Alcoholic Liver Disease (ALD) casts for 4% of the death rate and 5% of DALYs, reported in European countries. A million deaths were reported in 2010, accounting for fibrosis and cirrhosis with alcohol, and among ten, one death is attributed to AH [2]. In the US population, a death rate of 5.5/per 100,000 was anticipated in 2010. AH is linked to 41% of the death rate in the European Union [3]. Having considerable advances in the ground of AH treatment, the existing treatment strategies have huge limitations like no impact on survival (Glucocorticoids), increased infection frequency within two months (Anti-TNF therapy), unsuccessful in treating (caspase inhibitors, probiotics), and reversal with increased seriousness making the treatment difficult [4].

In order to combat adverse events and enhance the epidemiology of AH, it is necessary to treat the life-threatening disease. In recent studies, alkaloids have shown clinical advancement. Majorly, capsicum species have been under examination for their wide variety of pharmacological applications like anti-inflammatory [5], anti-obesity, antioxidation [6], anti-carcinogenic, and lowering of lipid peroxidation [7].

Although it has an extensive spectrum of beneficial possibilities, it is unexplored because of its limitations, such as low oral bioavailability, hydrophobicity, gastric irritation, burning diarrhea, nausea, and vomiting [8]. Hence it is necessary to explore a formulation strategy to reduce the complications and improve the oral bioavailability of Capsaicin (CAP).

A natural polysaccharide, Chitosan (CS) has excellent microbial degradability, blood compatibility, bio-functionality, and water solubility characteristics. It is renowned for its several biomedical applications, such as the controlled delivery of hydrophobic drugs [9]. Molecular weight (5 kDa), high viscous nature, less solubility in biological fluids (pH 6.3 to 7.8), and low cell specificity have restricted the use of CS *in vivo* [10]. Chemical alteration of CS was a capable approach to confiscate the limitations, resulting in improved transfection effectiveness and targeting capacity.

Many studies have been conducted in recent years to use hydrophobic longer-chain fatty acid of SA to graft CS to form CS-grafted-SA (CS-g-SA); further, it self-aggregates to make polymeric micelles in aqueous solution [10]. Additional studies found that CS-g-SA micelles had a spatial organization with a multi-hydrophobic core and could be quickly up-taken by tumor cells [11, 12].

Utilizing "Design of Experiments" (DoE) is an innovative advance in optimizing and transmitting experimental factors. Simple experimental plans and statistical tools for information analysis can offer a huge advantage regarding the system under examination after a small number of experiments [13]. A statistical technique called Response Surface Methodology (RSM) is utilized for DoE and the construction of experimental models that link several interacting components [14]. Central composite designs (CCD) and Box-Behnken designs (BBD) are the two most often utilized designs in response surface modeling.

The current study is aimed to optimize the parameters for the synthesis of CS-g-SA by using DoE. The study includes process optimization, preparation, and evaluation of the polymeric micelles of CS-g-SA with CAP loaded [15].

MATERIALS AND METHODS

Capsaicin is obtained from AOS Products Private Limited, Ghaziabad. CS oligosaccharide with a degree of deacetylation of 85% and an M.

Wt. of 5 kDa and Dialysis membrane (3kDa) obtained from Himedia Laboratories Pvt Ltd., Mumbai, India, SA, 2,4,6-trinitrobenzene sulfonic acid (TNBS), N-hydroxysuccinimide (NHS, purity ≈ 98%), 1-ethyl-3-(3-dimethyl aminopropyl) carbodiimide (EDC, Purity 99%), 1-dodecyl-pyridinium chloride (DPC with purity 98%) obtained from Sigma Aldrich, New Delhi. Dimethylsulfoxide, ethanol, sodium bicarbonate, hydrochloric acid, Iodine, Potassium Iodide were obtained from SD Fine Chemicals, Hyderabad, and Millipore filter paper (0.45 µm) obtained from M/s Merck Specialities Private Limited, Mumbai, India.

Design of experiments

Quality by design (QbD) for product development

QbD is a methodical proposition for product improvement with pre-established targets, including previous knowledge, DoE, knowledge management through the product life cycle, and assessment of risk. In contrast to typical approaches, the QbD incorporates quality throughout the development process (quality analyzed after production) [16]. QbD comprises forming the superior grade targeted product outline and identifying the major quality features, vital material characteristics, and significant method parameters. In the current study, QbD was functional in risk assessment (cause and effect relationship) to recognize the variables that affect the CQAs, screening of variables, and optimization and embarking on design space.

QTPP and CQAs

The QTPP includes a likely sketch of the desired qualities of the finished product that guarantee its "effectiveness, safety, and quality." Recognizing QTPP is the initial step in QbD, followed by the recognition of CQAs [17].

Risk assessment entails examining many aspects of the final CQAs. In addition, the factors significantly impacting the CQAs have to be recognized [17, 18].

Synthesis of SA grafted CS copolymer

The CS-g-SA was synthesized by amidation method [19]. Briefly, molar ratio 0.001: 0.0001 of CS and SA (CS 100 µg and SA~ 95 mg) were dissolved in 20 ml of dimethylsulfoxide (DMSO). The resultant solution was sonicated (Sonics and Materials, Inc., Vibra cell VCX 750) for 15 min at 50 °C, further SA was activated by 1-ethyl-3-(3-dimethyl-aminopropyl) carbodiimide (EDC-50µg) in the presence of N-hydroxysuccinimide (NHS-0.06µg), and the reaction was conducted in a hot water bath (50 °C for 30 min) at 1000 rpm. The reaction mixture is maintained at 80 °C for 8 h to complete the reaction. The blend has brought to room temperature and stirred continuously for 24 h at 2000 rpm for the formation of the copolymer. The formed copolymer was subjected to dialysis (dialysis membrane-MWCO, 3.5 kDa) for 72 h using ultrapure water to remove unreacted stearic acid. Filtered the copolymer mixture through a 0.45 m Millipore filter, dried the residue in an oven, and then utilized the dried product for further characterization [19, 20].

Optimization of process parameters for the synthesis of CS-g-SA using CCD

CCD with three factors and four levels was used to synthesize CS-g-SA by taking independent variables: Reaction-Time (B), Reaction-Temperature (A), and Stirring-Speed (C). Twenty model tests were produced by "Design-Expert® 11.0 (Stat-Ease Inc., Minneapolis, Minnesota, USA)". Consequences of these attributes on CS-g-SA characteristics (responses Y1: particle size, Y2: practical yield) were screened [21, 22]. Conditions in accordance with experiments due to the trials are furnished in table 1.

Table 1: List of independent and dependent variables

Screening of significant factors for synthesis of CS-g-SA using CCD						
Independent variables			**Levels**			
Variable	**Name**	**Units**	**-1**	**+1**	**-α**	**+α**
A	Reaction temperature	°C	50	80	39.77	90.23
B	Reaction time	min	240	480	158.18	561.82
C	Stirring speed	rpm	400	1000	195	1205
Dependent variable			Goal			
Y1	Practical yield	%	Accelerate			
Y2	Particle size	nm	Decrease			
Screening of significant factors for the preparation of micelles using BBD						
Independent variables			Levels			
Variable		Units	Low	Intermediate	High	
A	Dialysis time	min	60	120	180	
B	Organic: Aqueous phase	v/v	1	2	3	
C	Stirring time	min	30	60	90	
Dependent variables			Goal			
Y1	Encapsulation efficiecny	%	Increase			
Y2	Particle size	nm	Decrease			

Characterization of CS-g-SA

Amino groups substitute degree (SD%)

The "2-4-6-trinitrobenzene sulfonic acid (TNBS)" method was employed to calculate SD% [11]. To solutions of CS and CS-g-SA at various concentrations, NaHCO3 (4%) and 0.1% TNBS (0.1%) were added progressively. After adding hydrogen chloride (2 mol/l), incubated the mixture for 2 h at 37 °C. By employing ultraviolet-visible spectrophotometry (Shimadzu SPD-10A, Japan) absorbance was recorded at 344 nm after 30 min ultrasonication for five batches B1-B5 with an increased molar ratio of CS: SA [21].

Critical micelle concentration (CMC)

CMC was determined using UV-Vis spectrophotometry at 366 nm with the iodine solubilization method. In the hydrophobic surrounding of CS-g-SA copolymer, I_3^- get is converted to I_2 to form potassium iodide [22]. Iodine (0.5 g; 1%w/v) and potassium iodide (1.0 g; 2%w/v) were solubilized in ultrapure water (50 ml) to form KI/I_2 solution (standard). The concentrations of CS-g-SA dilutions were prepared from 1.0 µg/ml to 100 µg/ml. At room temperature, dilutions were sonicated for 30 min with 25 µl of the standard solution, and the resulting mixtures were then kept in the dark for 12 h. The UV absorbance was measured at 366 nm (KI/I_2 standard solution), and a plot was drawn between the adsorption and CS-g-SA micelle concentration. The "pointed peak" in the absorbance of the graph indicates the CMC [23].

Preparation of micelle by active drug loading

In order to prepare micelle, 200 mg of CS-g-SA were dissolved in 200 ml of ultrapure water using a sonicator (Sonics and Materials, Inc., Vibra cell VCX 750) in an ice bath for 30 min, 20 cycles (400 W, pulse on 2.0 s, pulse off 3.0 s) [24]. With constant stirring, CAP was added dropwise to the empty micelle solution after being dissolved in DMSO (10 ml) [25]. Using 10 volumes of ultrapure water, the CAP-loaded micelles were introduced to a dialysis bag (MWCO, 3.5 kDa). The triple distilled water was refreshed every 30 min to remove the free drug and DMSO. Finally,

CAP-loaded CS-g-SA (CAP-CS-g-SA) micelles were collected in the dialysis bag, lyophilized and used for further study [11].

Optimization of process parameters for the preparation of micelles using BBD

Encapsulation efficiency (EE) and particle size (PS) of CAP-loaded micelles were used as the response variables in a BBD study to examine the effects of three controlled factors, including dialysis time (A), the volumetric ratio of organic to water phase (B), and stirring time (C) [22]. The BBD got engaged to optimize and examine main, interactive, and quadratic effects [26]. Seventeen experiments were produced by "Design-Expert® 11.0 (Stat-Ease Inc., Minneapolis, Minnesota, USA)". Conditions following experiments due to the trials are furnished in table 1.

Characterization and evaluation of micelles

Encapsulation efficiency

The filtration method determined the EE of CAP in the micellar system [27]. To remove non-encapsulated CAP, CAP-CS-g-SA micelle (5 mg/ml) was diluted with distilled water and passed through a 0.22 m filter membrane. The methanol was then thoroughly combined with 0.1 ml of the filtrate to obtain a volume of 10 ml. Using a UV-Vis spectrophotometer with a wavelength of 282 nm, the amount of the encapsulated CAP was quantified. The following equation can express the loading capacity and EE % calculations of CAP-CS-g-SA micelle [28].

$$\text{Encapsulation efficiency}(\%) = \frac{\text{Amount of drug after filtration}}{\text{Total amount of drug in the sample}} \text{X } 100$$

$$\text{Loadingcapacity} = \frac{\text{Total amount of drug} - \text{free amount of drug}}{\text{Nanoparticle weight}} \times 100$$

Particle size, zeta potential, and polydispersity index

Using the Malvern particle size analyzer (Master sizer 2000, Malvern, UK), the dynamic light scattering technique was employed to assess the particle size distribution of the blank and CAP-CS-g-SA micelles. For zeta potential, diluted micelles dispersions were placed in polystyrene electrophoretic cells. An "Au-plated electrode (U shape)" cell was used to measure the micelle's zeta potential at a count rate of 250 particles per second at a temperature of 25 °C. Experiments were repeated thrice [29].

Surface morphology

Under transmission electron microscope JEM 2100 (JOEL, Tokyo, Japan) CAP, blank, and CAP-CS-g-SA micelles morphology was observed. On top of a film-coated Cu grid designated with a 2% (w/v) solution of "phosphotungstic acid," one drop of micelle was applied. To enhance the contrast, it was allowed to dry. Samples were analyzed at 45000× intensification using transmission electron microscopy [30].

^{1}H nuclear magnetic resonance (^{1}H NMR)

To confirm the synthesis of the CS-g-SA and to analyze CAP-CS-g-SA micelles ^{1}H NMR spectrum was used. ^{1}H NMR spectra for CAP, SA, CS, SA-g-CS, and CAP-SA-g-CS were established (Varian Unity-Plus 400 NMR Spectrometer in $CDCl_3$) to verify the formation of CA-g-SA [27]. ^{1}H NMR spectra were recorded in DMSO.

Fourier transmission infrared spectroscopy (FTIR)

The CAP, CS, SA, CS-g-SA, and CAP-SA-g-CS FTIR spectra were obtained utilizing KBr (Potassium Bromide) disc process (Tensor 27, FT-IR Spectrophotometer) with a range of 4000-600 cm^{-1}.

X-ray diffraction pattern

Using a Philips X-ray diffract meter (PW-1710) with a graphite monochromator and Ni-filtered Cu Kα radiation at a scan speed of 1 °2 θ min^{-1}, 20 m A current, and 30 kV voltage, the "X-ray diffraction pattern" of CAP and CAP-SA-g-CS was captured [31].

Differential scanning calorimetry

The Perkin Elmer STA 8000 Thermal Analyzer was used to analyze CAP and CAP-SA-g-CS. An apparatus that had been calibrated using indium was used to measure the melting point and heat of fusion. At a rate of 10 °C/min, the temperature range of 30-400 °C was activated. Regular Al (aluminum) Perkin-Elmer sample pans were utilized, and an empty pan was used as a standard. A triplicate examination was conducted on samples (5 mg) using nitrogen purge [32].

Hemolysis test

A hemolysis study was performed by isolating erythrocytes from human blood (heparinized) using centrifugation (2,800 rpm, 5 min). In PBS-phosphate buffer saline (pH 7.4) established erythrocytes lump be re-suspended. These washing steps have to be repetitive (thrice). Separated erythrocytes re-suspended in 0.9% NaCl, resulting in 2% (v/v) of RBC suspension [33]. After incubating the suspension (1.8 ml) with the test samples (0.2 ml) for 0.5 h at 37 °C, centrifugation was performed (2,800 rpm, 5 min). Percent hemolysis of supernatant was calculated using a UV–Vis spectrophotometer at 545 nm. Distilled water used as a positive control (100 percent hemolysis) and PBS (pH 7.4) as a negative control (no hemolysis). The following equation was used to determine the hemolysis % [34].

$$\%\ \text{Hemolysis} = \frac{\text{ABS}_{\text{Sample}} - \text{ABS}_0}{\text{ABS}_{100} - \text{ABS}_0} \text{X } 100$$

WhereABS_0-Absorbance at 0% hemolysis

ABS_{100}-Absorbance at 100 % hemolysis

***In vitro* drug release**

Dialysis was used to accomplish *in vitro* CAP release from micelles [35]. Free CAP and CAP-SA-g-CS (10 mg) were placed in dialysis bags into containers with 100 ml release medium (pH 7.4, PBS). Two sets were placed additionally. Containers were swirled at 37 °C at a rate of 300 rpm/min. At each time point, a release medium (5 ml) was drawn. An equal measure of the medium was refilled to keep sink conditions. CAP concentration present in the release medium was estimated by UV–Vis spectrophotometer at 282 nm (λ_{max} of CAP), and the accumulative release percentage of CAP was calculated [27].

Drug release kinetics

The *in vitro* release data were integrated into kinetic models (Korsemeyer Peppa's, Higuchi's, first order, and zero zero-orders). The fitting curve technique understood CAP release through micelle formulation [36]. Results obtained through *in vitro* release studies were verified with different kinetic equations.

Zero order Model:

$$Q_t = Q_0 + K_0 t$$

Q_t-Quantity of drug dissolved in time t,

Q_0-Original quantity of drug

K_0-Zero order release constant

First order Model:

$$\ln(Q_\infty - Q_t) = \ln Q_0 + Kt$$

Q_t-Quantity of drug dissolved in time t,

Q_0-Original quantity of drug

Q_∞-Amount released in time ∞ (100 % drug release)

K-First order release constant.

Higuchi model:

$$Q_t = k_H t^{\frac{1}{2}}$$

Q_t-Quantity of drug dissolved in time t,

k_H-Higuchi dissolution constant

Korsmeyer–Peppas Model (power law):

$$\frac{Q_t}{Q_\infty} = K_K t^n$$

or

$$\log Q_t = \log K_k + n \log t$$

Q_t-Amount of drug dissolved in time t,

Q_∞-Amount released in time ∞,

K_k-Rate constant

n-Diffusional exponent [37].

Stability of micelles

For three months, the stability of CAP-loaded micelles was assessed at three different temperatures (4, 25, and 40 °C). The content of CAP, EE, and mean particle size of CAP-CS-g-SA micelles was established on the 1st, 15th, 30th, 45th, 60th, and 90th day [38].

Statistical analysis

Results were articulated as mean±SEM, n=3. Statistical analysis is done by one-way ANOVA, which is followed by Dunnett"s multiple comparison tests. Results were computed for statistical analysis y using Origin pro (V 8.0). The value $p<0.01$ was regarded as statistically considerable.

RESULTS AND DISCUSSION

Design of experiments

Quality by design (QbD) for product development (QTPP and CQAs)

This study aimed to organize CS-g-SA (carrier system) for hepatocytes intake and improve hydrophobic CAP's oral bioavailability. Recognizing CQAs is an initial step in the QbD method and the organization of CQAs in the accepted range ensures the attainment of QTPP [39]. Practical yield and particle size (Synthesis of SA grafted CS copolymer), EE, and particle size (Micelle formulation of CAP-CS-g-SA) have opted as CQAs (table 2). Size affects the cellular uptake where minor particles have enhanced penetration and size reductions confer drug availability in the dispersed form, which enhances the dissolution. Practical yield is the quantity of a product obtained from a chemical reaction. The EE is the quantity of drug that is included in the micelles. Elevated EE is desired to have advantages [40].

Table 2: QTPP and CQAs identification

QTPP	Target	Justification
Formulation	Nanosized Micelles	With improved bioavailability, decreased toxicity, prolonged release, lengthy circulation, and precisely targeted administration, polymeric micelles have shown promise as nanocarriers for the delivery of difficult-to-formulate active moieties.
Stability	Up to 30 d after formulation, there was not a noticeable sign of aggregation	It is important to keep the same particle size since it affects the formulation's effectiveness.
Pharmacokinetics	Ought to be improved	For increased bioavailability
Route of administration	Oral	The oral bioavailability of the marketed product is the main objective.
CQA	Target	Justification
Particle size	Average particle size below 200 nm	The increase in surface area associated with nanoscale size improves solubility and dissolution, which improves bioavailability and reduces pharmacokinetic variance.
Encapsulation efficiency (EE)	Higher	Increased drug loading in the carrier system is ensured by greater EE.
Practical yield	Higher	Higher the practical yield better availability of CAP

Risk assessment and identification of CMAs and CPPs

The initial step in early risk assessment was to create an Ishikawa (fishbone) diagram (fig. 1). It displays how each variable affects the CQAs. Only the significant variables out of all the other parameters were examined for screening trials [41].

Synthesis of CS-g-S A copolymer

By amidating the-NH2 groups of CS with the -COOH groups of SA while employing NHS and EDC, the CS-g-SA was generated [21]. The COOH of SA gets reacted with EDC to form an unstable intermediate. A subsequent reaction between the obtained intermediate and EDC produced an active ester [23]. CS-g-SA is formed when the active ester forms an amide bond (amidation) with the primary amino group of CS [4].

Optimization of process parameters for the synthesis of CS-g-SA copolymer

CCD was used to optimize three components with four levels for twenty experiments. Utilizing "Design-Expert® 11.0 software (Stat-Ease Inc., Minneapolis, MN, USA)," the data was processed to provide 3D response surface plots, regression coefficients, and analysis of variance (ANOVA).

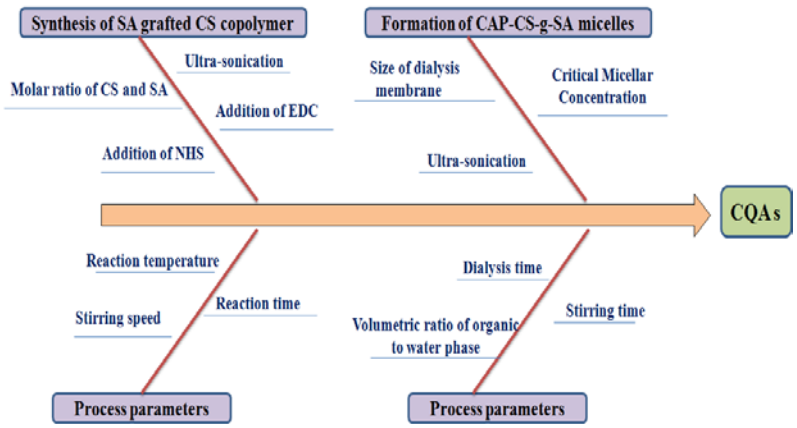

Fig. 1: Cause and effect relationships are shown in an Ishikawa (fish-bone) diagram for the creation of capsaicin-loaded, stearic acid-grafted chitosan micelles

Practical yield

The equation shows how the process variables A, B, and C work together and how much they affect the practical yield % (Y1), as shown in the equation.

$$\text{Practicalyield (Y1)} = 58.2 + 19.1A + 4.8B + 4.3C$$

Fig. 2(a) presents essential effects, quadratic effects, and interface effects of stirring speed (C), time (B), and temperature (A) on Y1. It presents that A had a significant influence on Y1. B and C have a modest influence on Y1. Y1 increased from 24.6 to 89.4 %, indicating the need to maintain appropriate conditions for synthesizing CS-g-SA. Sufficient temperature causes dislocation multiplication. Further, increasing dislocation density leads to polymer linking [42]. Association among Y1 and A and B was additionally presented using a response surface plot and contour plot. The impact of A and B on Y1 at the set point of C is shown in fig. 2(b) and 2(c) (700 rpm). Experiments showed that low temperature (50 °C) prevented the CS-g-SA formation, while high temperature (>100 °C) led to the development of reticulate. It failed to generate the highest possible product yield with shorter reaction times.

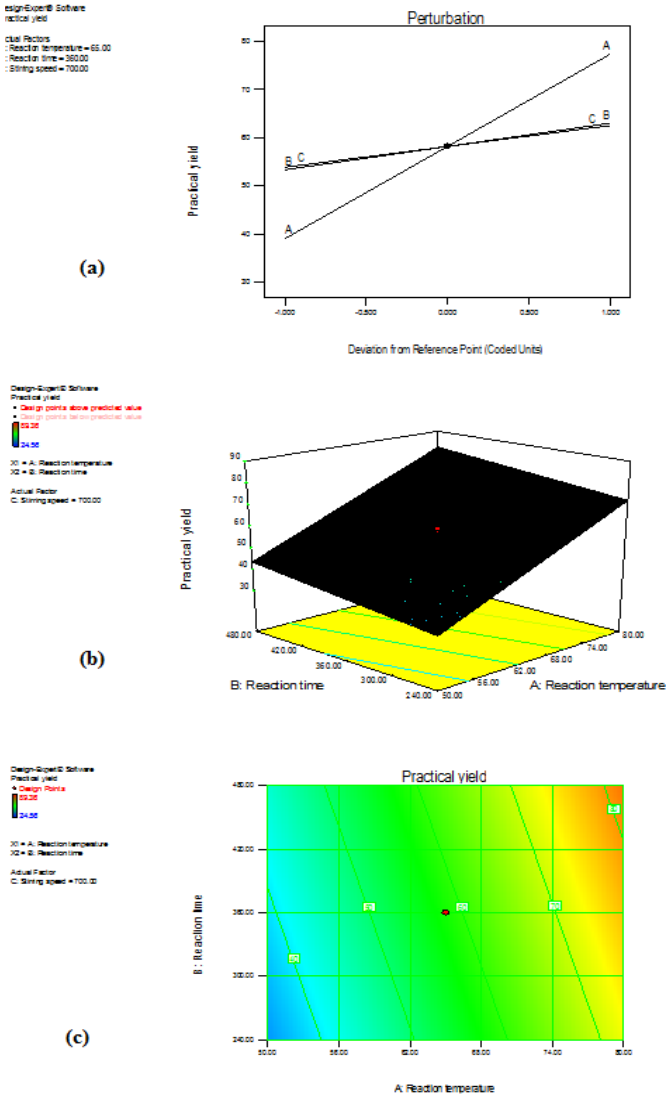

Fig. 2: (a) Perturbation plot presenting effect stirring speed, reaction time, and reaction temperature on practical yield; (b) Response surface plot presenting control of reaction time and reaction temperature on practical yield; (c) Contour plot presenting the control of reaction time and reaction temperature on practical yield

Particle size

The polynomial equation represents the influence of reaction stirring speed (C), time (B), and temperature (A) on average particle size (Y2).

$$\text{Mean particle size(Y2)} = 157.5 - 10.9\,A - 22.4\,B - 48.9\,C + 9.6\,AB + 7.5\,AC + 12\,B^2 + 34\,C^2$$

It was examined that the copolymers particle size fell between 126.4 and 336.5 nm.

Fig. 3(a) presents crucial effects, relations effects, and quadratic influence of reactions A, B, and C on Y2. The fig. presents that C has a major, B has a modest, and A has a minor influence on Y2. Association among dependent and independent parameters is additionally elaborated using response surface and contour plots, as presented in fig. 3(b) and 3(c). The fig. illustrates that C is oppositely proportionate to the Y2, an incline in C (195 to 1000 rpm) leads to a decline in Y2 (336.5 to 126.4 nm). Moreover, Y2 is negatively impacted by the increase in A. A decline in Y2 was caused by an increase in A (40 °C to 80 °C) (175.4-138.7 nm). Similar to A, B also affects Y2 negatively. A major interaction among the independent parameters has been identified. Contour plots in fig. 3(d) and 3(e) present interaction among A and B on average Y2 at a set point of C (700 rpm). In the same manner, the interaction among A and C on mean Y2 at a preset point of D (360 min). The generated polymer's particle size is majorly impacted by stirring speed.

The maximum function value was attained at A: 80 °C, B: 480 min, and C: 946 rpm. Five batches of SA-g-CS were synthesized under ideal conditions with varying molar concentrations (1:0.1, 1:0.2, 1:0.3, 1:0.4, and 1:0.5). Based on the outcomes from preliminary testing, the range and level of independent parameters were established [43]. The dependability of the developmental process in measuring the operating parameters (synthesis of CS-g-SA) is presented in table 3.

Table 3: Optimized values acquired by the constraints applied on Y1 and Y2

Independent variable	Nominal values	Anticipated values		Observed values		
		Practical yield (Y1)	Particle size (Y2)	Batch	Practical yield (Y1)	Particle size (Y2)
Reaction temperature (A)	80	85.7	134.7	B1	83.6	138.8
				B2	85.8	137.1
Reaction time (B)	480			B3	86.2	135.3
				B4	86.7	131.2
Stirring speed (C)	946.5			B5	87.1	128.5

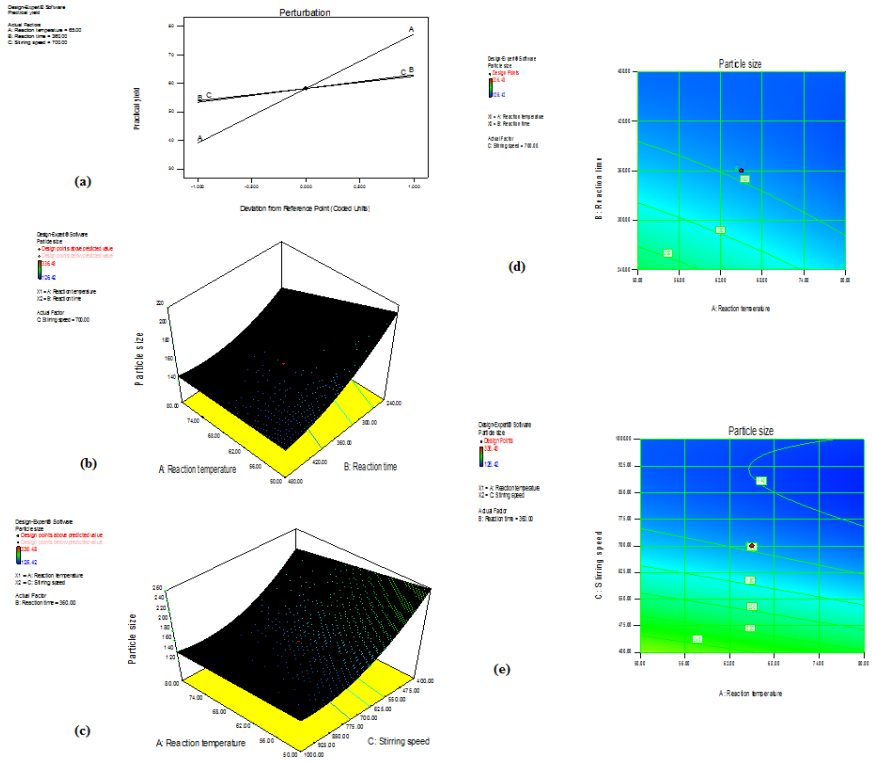

Fig. 3: (a) Perturbation plot presenting the impact of stirring speed, reaction time, and reaction temperature on particle size; 3(b) Response surface plots presenting the interactions among the reaction time and reaction temperature at steady stirring speed; 3(c) Response surface plots indicating the interactions among stirring speed and reaction time at steady reaction temperature; 3(d) Contour plots showing the interactions among the reaction time and reaction temperature at steady stirring speed; 3(e) Contour plots showing the interaction among stirring speed and reaction time at the steady reaction temperature

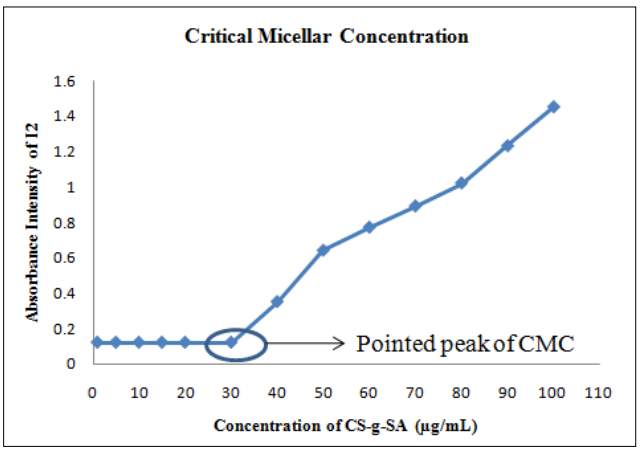

Fig. 4: Graph for determination of CMC value of CA-g-SA, Note: Critical Micellar Concentration (CMC) of CS-g-SA copolymer was identified by the Iodine method. The CMC graph plotted for dilutions of CS-g-SA and absorbance intensity of I_2 at 366 nm

Characterization of CS-g-SA (CMC and SD%)

A graph is drawn among concentration (CS-g-SA polymer) and their related absorbance at 366 nm (fig. 4). CS-g-SA CMC value is 30.3µg/ml. The CMC and the size of the polymer's particles were found to decrease as the SD% increased [43].

Preparation of micelle by active drug loading

The created CS-g-SA was dissolved in distilled water using ultrasonic, and at first, empty micelles developed as a result of their natural tendency to self-aggregate in aqueous environments. By active loading, the drug was stably entrapped in the core of the micelles and resulted in nanosized micelles [38].

Optimization of process variables for the preparation of micelles

A 3-factor, 3-level BBD was utilized, and 17 runs were performed. Resultant data were analyzed through "Design-Expert® 11.0 software (Stat-Ease Inc., Minneapolis, MN, USA)" to find regression equations, analysis of variance, and regression coefficients [44]. ANOVA, lack of fit, and multiple regression coefficients (R2) values were used to determine the appropriateness of the second-order quadratic model into which the findings were fixed.

Encapsulation efficiency

In micelles, drug encapsulation is insignificant for improving the solubility and bioavailability of CAP [44]. The EE (Y1) of micelles was in an array of 50.4-69.2 %. The quadratic model generated for EE was considerable, with an F-value of 166.6. The individual variables A, B, interactive term (AB), and quadratic terms A^2 and B^2 significantly influenced EE with a P value<0.05. The "Lack of Fit F-value" (3.49) suggests that it is not crucial. The factorial equation for EE indicated that the effect of A is more considerable than B with a good correlation coefficient (R^2) and adjusted R^2 values for the model 0.98697 and 0.98104, respectively.

The EE increased (50.4 to 69.2%) when the dialysis period (A) increased from 60 to 120 min. EE is escalated from 50.4 to 57.3 % at lower points of A. At higher levels of A, EE decreased from 61.12 to 54.34 %. As the ratio of the organic to the aqueous phase (B) increases from 1 to 2, the EE increased from 50.4 to 69.2 %. At lower points of B, EE escalated from 50.4 to 64.3 %. An antagonistic quadratic impact was seen at higher values of B. At higher levels of B, EE decreased from 65.5 to 54.3 %. Perturbation, 3D surface, and contour plots were constructed to show independent parameters' significant and collective influence on EE. Individual influences of A and B on EE were presented in the perturbation plot. Fig. 6(a) demonstrates that A has a major consequence on EE followed by B with a modest outcome. The collective effect of AB at a steady level of C on EE is depicted in fig. 6(b) and 6(c). Y1 for all batches was found to be in the range of 50.38-69.18%.

Particle size

Particle size is a significant quality control assessment for nano-micelles. Size distribution is a significant factor concerning micelles' physical properties and stability. It is also a critical aspect that impacts permeation and retention through different tissues and related organs [45]. Micelles had particles that ranged in size from 156.46 to 333.94 nm. The polynomial model depicts that all parameters considerably influence micelle particle size.

The quadratic model's F-value of 8510.91 indicated its relevance. Individual variables (A, Band C), interactive term (BC), and quadratic terms A^2 and B^2 were found to have a significant influence on particle size (P<0.05). The "Lack of Fit F-value" (0.42) suggests that it is not noteworthy. A "Lack of Fit F-value" of this magnitude has an 81.7% chance of occurring due to noise. The factorial equation for particle size indicated that the influence of C is far greater than the effects of A and B with good R^2 and adjusted R^2 values for the model 0.99749 and 0.99554, respectively.

As the A increases from 60 to 120 min, the Y2 also rises (178.1 to 333.9 nm); variations of Y2 incline at lower levels of A. (178.1 to 312.5 nm). Higher A concentrations reduced particle size from 297.8 to 156.5 nm. As the ratio of the organic to the aqueous phase (B) increases from 1 to 2, the particle size increases from 182.8 to 312.5 nm. At lower amounts of B, particle size values inclined from 182.7 to 333.9 nm. At higher amounts of B, particle size decreased (299.2 to 186.9 nm). As C increases from 30 to 90 min, the particle size is reduced from 333.94 to 156.46 nm. At lower amounts of C, Y2 declined from 333.9 to 297.8 nm.

Similarly, at higher amounts of C, Y2 declined to 156.5 nm. The perturbation plot depicted the independent impacts of A, B, and C on particle size. Fig. 7(a) demonstrates that C has the greatest impact on particle size, whereas B and A have the least. The quadratic and collective impacts of independent factors were explicated by 3D response surface and contour plots. Fig. 7(b) and 7(c) show the interaction impact of A and B on particle size at a stable stage of C. Fig. 7(d) and 7(e) show the interaction impact of B and C (BC) on particle size at the steady state of A. The range for Y2 was 156.5-333.9 nm.

Characterization and evaluation of micelles

EE, zeta potential, particle size, and polydispersity index

The results of EE, zeta potential, particle size, and polydispersity index values are shown in Table 5. The EE of micelle was satisfactory and loading capacity was found to be 9.4±3%. The particle size of micelles was similar with lower polydispersity indices. Higher zeta potential values represent increased storage stability of micelles [46].

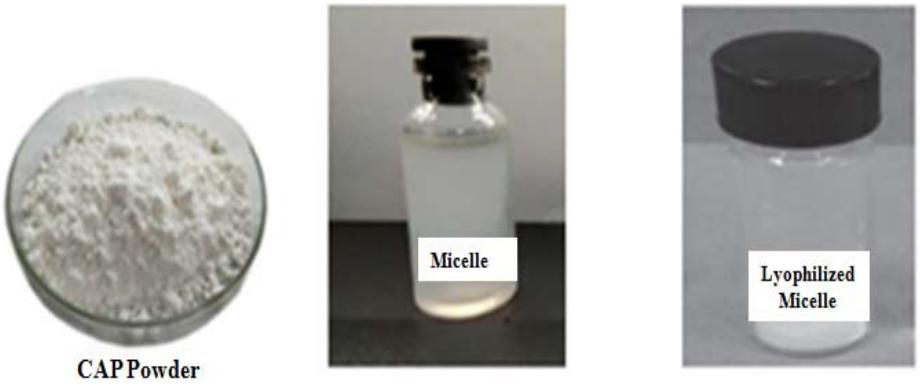

Fig. 5: Samples of CAP, CAP-CS-g-SA micelle and lyophilized micelle, Note: CAP: Capsaicin; CS: Chitosan; SA: Stearic acid

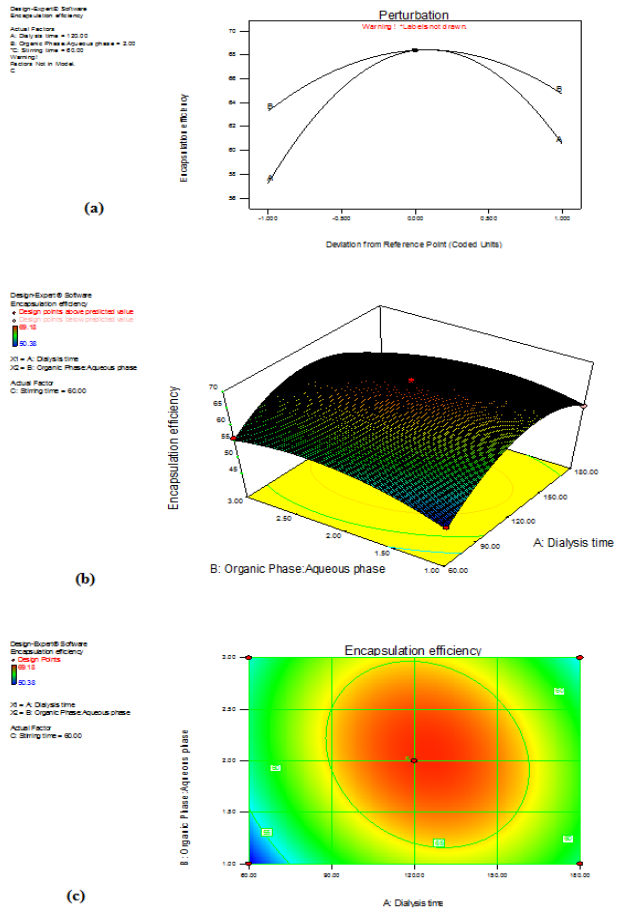

Fig. 6: (a). 2D Perturbation plot-Effect of dialysis time and organic: Aqueous phase on EE; 6(b) 3D-response surface plot presenting the interactive effect of dialysis time and Organic: Aqueous phase on EE at a steady level of stirring time; 6(c) Contour plot presenting the interactive effect of dialysis time and Organic: Aqueous phase on EE at a steady level of stirring time

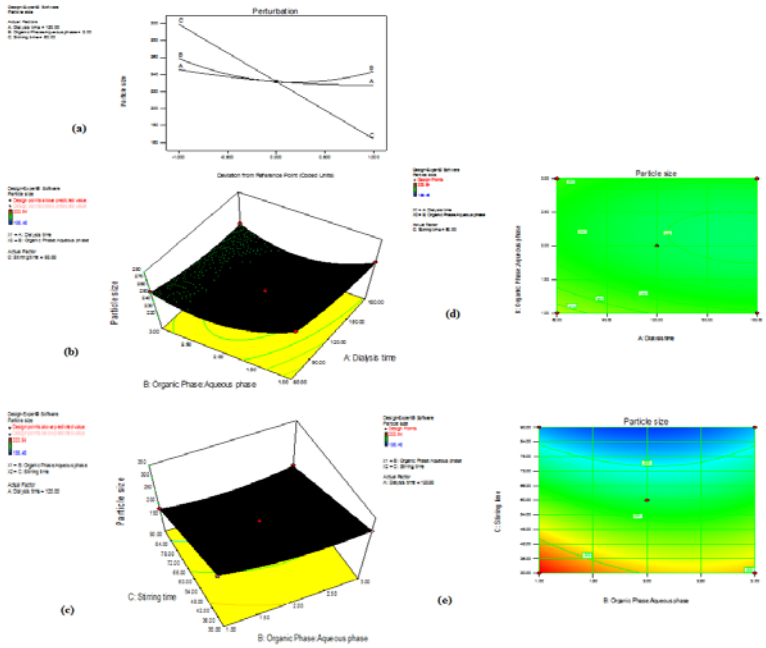

Fig. 7: (a). 2D perturbation plot–influence of dialysis time, organic: aqueous phase and stirring time on particle size; 7(b) 3D-response surface plot presenting the interactive influence of dialysis time and organic: aqueous phase on particle size at a steady level of stirring time; 7(c) 3D-response surface plot presenting the interactive influence of organic: aqueous phase and stirring time on particle size at a steady level of dialysis time; 7(d) Contour plot indicating the interactive effect of dialysis time and organic: aqueous phase on particle size at a steady level of stirring time; 7(e) Contour plot presenting the interactive effect of organic: aqueous phase and stirring time on particle size at a steady level of dialysis time

Table 5: Optimal setting acquired by restricting response parameters

Independent variables	Optimized values	Predicted values		Batch	Actual values*			
		EE (Y1) %	Particle size (Y2) nm		Encapsulation efficiency (Y1) %	Particle size (Y2) nm	ZP (mV)	Polydispersity index
Dialysis time	128 min	68.5	163.2	F1	67.6	171.2±10.5	26.5±2.1	0.27±0.005
Organic phase: Aqueous phase	2.01			F2	68.1	168.6±8.1	23.5±1.8	0.31±0.005
Stirring time	90 min			F3	68.4	166.5±6.7	28.3±3.1	0.2±0.005

*Values are shown as the mean±standard deviation, with n=3.

Surface morphology

"A transmission electron microscope" was used to examine the surface morphology of produced micelles. TEM image revealed the well-formed spherical and uniform-sized micelles in a size array of 150-200 nm (fig. 8). Samples were analyzed at 45000× intensification using transmission electron microscopy.

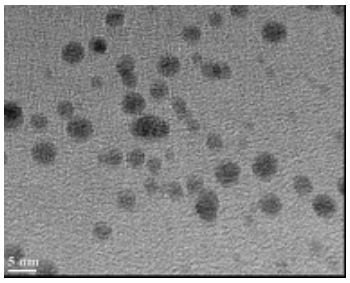

Fig. 8: TEM image (45000× intensification) of capsaicin-loaded micelles

^{1}H NMR and FTIR

The structures of the CAP and polymers were established using ^{1}H NMR and FTIR. Fig. 9(a) shows CAP-CS-g-SA, CS-g-SA, SA, CS, and CAP ^{1}H NMR spectra. The ^{1}H-NMR spectra of CS-g-SA revealed a strong signal at d=1.0 ppm, which was attributed to SA's -CH_2-. The methyl and methylene hydrogen of the stearate group might be responsible for the 0.9 and 1.0 ppm chemical shifts. As a result, it was considered that SA had successfully been grafted onto CS [45]. The distinctive peaks at 0.90 and 1.31 ppm in the ^{1}H NMR spectra of the CAP can be traced to the CAP's CH_3 and CH_2 protons, respectively. In both polymer conjugates, all differentiating CAP peaks dissipated, suggesting the incorporation of the drug in the hydrophobic micellar core [21].

Fig. 9(b) shows the FTIR spectra of CAP-CS-g-SA, CS-g-SA, SA, CS, and CAP. In the grafted polymer spectra, the typical peaks of CS amide bands I and II were displaced to 1640 cm^{-1} and 1560 cm^{-1}, indicating the amide band between SA and CS. The disappearance of CAP's prominent characteristic peaks indicates the drug's internalization within the polymer's hydrophobic core [10].

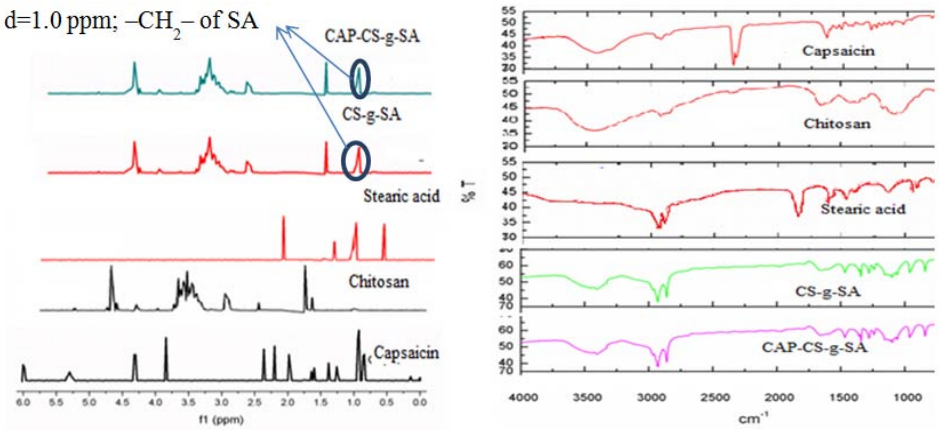

Fig. 9(a).^{1}H NMR spectra of CAP, CS, SA, CS-g-SA and CAP-CS-g-SA using DMSO solvent; 9(b) FTIR spectra of CAP, CS, SA, CS-g-SA and CAP-CS-g-SA

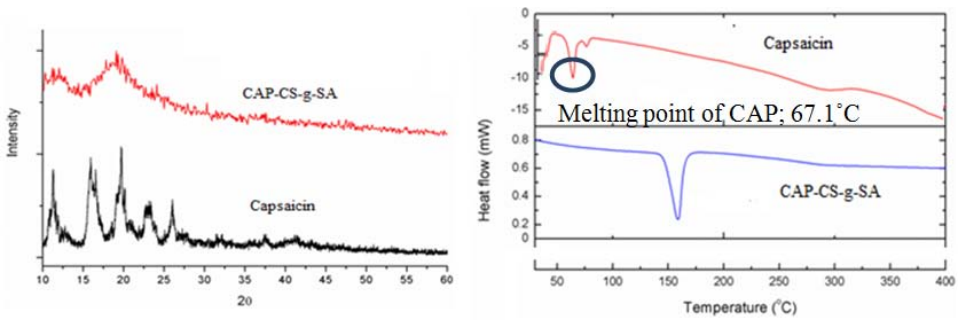

Fig. 10: (a). X-ray diffraction patterns of CAP and CAP-CS-g-SA; (b). DSC curve of CAP and CAP-CS-g-SA, Note: CAP: Capsaicin; CS: Chitosan; SA: Stearic acid
Note: CAP: Capsaicin; CS: Chitosan; SA: Stearic acid

XRD and DSC

XRD and DSC were used to characterize the free CAP and freeze-dried CAP-SA-g-CS micelles in the solid state. Fig. 10(a) displays the XRD patterns of powder samples. The CAP diffraction peaks demonstrated the drug's crystalline form. In contrast, the distinctive CAP diffraction peaks dissipated in the freeze-dried micelle products, showing the complex's creation represented a new solid-state (fig. 10a) [31].

The melting point of CAP is shown by an endothermic peak (67.1 °C) on its DSC curve. The endothermic peak of the CS-g-SA DSC curve is represented at 159.12 °C. The interaction with the polymer conjugates was demonstrated by the practically complete disappearance of CAP's distinctive melting peak. These findings suggested that the freeze-dried product's CAP and polymers interacted vigorously (fig. 10b) [38].

Hemolysis test

Non-toxicity of the formulation is a compulsory requirement; hence hemolytic performance was determined to identify the safety and biocompatibility of CAP-CS-g-SA and CS-g-SA micelles [31]. Fig. 11 shows the hemolytic activity of plain and drug-loaded micelles. Plain micelles' aqueous suspensions (5 mg/ml) were non-hemolytic. Drug-embedded micelles also showed a safety profile with erythrocytes [37]. Optical microscopic images at 400x magnification presented the existence of erythrocytes following incubation with plain and drug-loaded micelle, thus proving its intactness and safety [24].

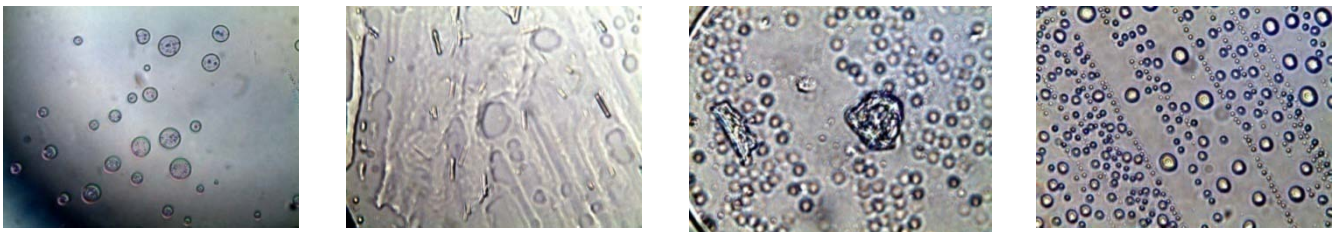

(a) **(b)** **(c)** **(d)**

Fig. 11: Photomicrographs (400x magnification) of erythrocytes treated with 11(a) PBS; 11(b) SLS; 11(c) SA-g-CS; 11 (d) CAP-SA-g-CS
Note: CAP: Capsaicin; CS: Chitosan; SA: Stearic acid; PBS: Phosphate Buffer Saline; SLS: Sodium Lauryl Sulfate

***In vitro* drug release**

Its pharmacokinetic attributes might be altered by the drug release performance [48]. Using the dialysis approach, the drug release pattern from micelles was identified. Drug release plots were constructed as shown in fig. 12. Almost all of the free CAP was distributed in the course of 6 h (99.48±2.56%). Drug-loaded micelles released CAP with a slower, more consistent release pattern. Micellar formulation released 86.8±1.92% of CAP in 24h, indicating that the micelle accomplished the formation of a more rigid hydrophobic core [21].

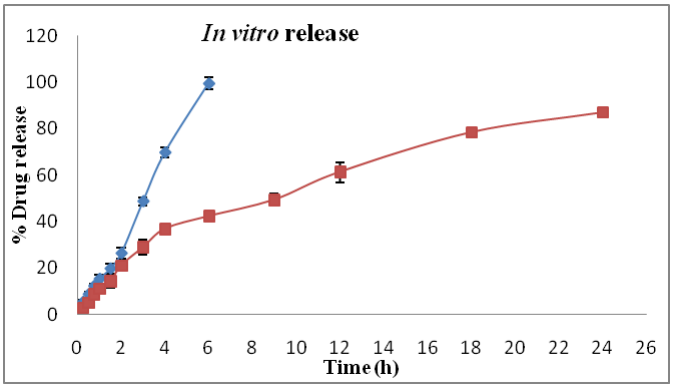

Fig. 12: *In vitro* drug release of Capsaicin and CAP-CS-g-SA (Capsaicin loaded stearic acid grafted chitosan micelle)
Note: Values are shown as the mean±standard deviation, with n=3

Drug release kinetics

To determine order and CAP release pattern, multiple kinetic equations were generated with drug release information for produced micelles [38]. According to the data, first-order kinetics has a regression coefficient value that is approximately 1. Hence it is discussed that the dissolution rate is directly proportional to the concentration of the drug [24]. In addition, by converting the data into a variety of mathematical models, including Higuchi and Korsmeyer-Peppas plots, the findings from the dissolution experiments indicate the possibility of comprehending the drug release strategy. According to the Higuchi model, the regression coefficient result is almost unity, suggesting that the mechanism by which drugs are released from the insoluble matrix as a square root of time-reliant process based on the Fickian diffusion Equation [48].

Stability of micelles

For three months, the storage stability of optimized CAP-loaded micelles was investigated at three different temperatures (4, 25, and 40 °C). Drug content, EE, and particle size of CAP micelles at the 0^{th}, 15^{th}, 30^{th}, 45^{th}, 60^{th}, and 90^{th} day were evaluated. No noteworthy alteration in drug quantity was noted at all temperatures. The EE hardly changed at 4 °C and 25 °C, signifying that micelles could shield CAP from deterioration or degradation [47]. The EE significantly reduced at higher temperatures, indicating the disruption of micelle structure at higher temperatures [46]. Furthermore, as storage time passed, the mean particle diameter gradually inclines. This might be connected to the dynamic micellar deconstruction and re-aggregation process that results in a somewhat established micellar system [49]. During the stability

experiment, CAP micelles' polydispersity index values were below 0.3, indicating the homogenous size allocation in the formulation.

CONCLUSION

In this study, we synthesized CS-g-SA copolymer and prepared polymeric micelles by optimizing the process parameters with CCD and BBD. QbD was productively functional for CAP-loaded polymeric micelles development. It was identified that the critical element affecting practical yield was the reaction temperature, while the main component affecting particle size was stirring speed. In contrast, reaction time and temperature showed an influence on EE%. The CMC and particle size of the polymer dropped as the SD% increased. The successful grafting of CAP-CS-g-SA was validated by FTIR, ^{1}H NMR, XRD, and DSC measurements. The hemolysis test has proven that the micelles were biocompatible. CAP-CS-g-SA micelle is an intriguing approach to enhance the bioavailability and controlled release of highly hydrophobic CAP and further *in vivo* studies would be evident for the treatment of AH using CAP-CS-g-SA. The present study is further planned to conjugate the copolymer with ligand for targeted delivery of CAP into hepatic cells.

ACKNOWLEDGMENT

The authors thank GITAM School of Pharmacy, GITAM Deemed to be University, Hyderabad, for their continuous support in encouraging, motivating, and providing "Design-Expert® 11.0 software (Stat-Ease Inc., Minneapolis, MN, USA)".

FUNDING

This research received no external funding.

AUTHORS CONTRIBUTIONS

M. K. S. S. completed the research work, execution, and writing and did the work plan, review, and corrections. Both authors agree with the submission and publication. All authors have read and agreed to the published version of the manuscript.

CONFLICTS OF INTERESTS

No conflict of interest

REFERENCES

1. Hughes E, Hopkins LJ, Parker R. Survival from alcoholic hepatitis has not improved over time. PLOS One. 2018 Feb;13(2):e0192393. doi: 10.1371/journal.pone.0192393, PMID 29444123.
2. Mitra S, De A, Chowdhury A. Epidemiology of non-alcoholic and alcoholic fatty liver diseases. Transl Gastroenterol Hepatol. 2020;5:16. doi: 10.21037/tgh.2019.09.08, PMID 32258520.
3. Singal AK, Louvet A, Shah VH, Kamath PS. Grand rounds: alcoholic hepatitis. J Hepatol. 2018 Jun;69(2):534-43. doi: 10.1016/j.jhep.2018.05.001, PMID 29753761.
4. Gao B, Bataller R. Alcoholic liver disease: pathogenesis and new therapeutic targets. Gastroenterology. 2011 Sep;141(5):1572-85. doi: 10.1053/j.gastro.2011.09.002, PMID 21920463.
5. Sukmanadi M, Effendi MH. The protective effect of capsaicin (Capsicum annum l) against the induction of aflatoxin b1 in hepatocytes: a study of liver histopathology in mice (mus musculus). Res J Pharm Technol. 2021 Feb;14(2):813-6. doi: 10.5958/0974-360X.2021.00143.8.
6. Koneru M, Sahu BD, Mir SM, Ravuri HGora, Kuncha M, Mahesh Kumar JM. Capsaicin, the pungent principle of peppers, ameliorates alcohol-induced acute liver injury in mice via modulation of matrix metalloproteinases. Can J Physiol Pharmacol. 2018 Apr;96(4):419-27. doi: 10.1139/cjpp-2017-0473, PMID 29053935.
7. Singh S, Uddin M, Khan MMA, Singh S, Chishti AS, Bhat UH. Therapeutic properties of capsaicin: a medicinally important bio-active constituent of chilli pepper. Asian J Pharm Clin Res. 2022 Jul;15(7):47-58. doi: 10.22159/ajpcr.2022.v15i7.44405.
8. Rollyson WD, Stover CA, Brown KC, Perry HE, Stevenson CD, McNees CA. Bioavailability of capsaicin and its implications for drug delivery. J Control Release. 2014;196:96-105. doi: 10.1016/j.jconrel.2014.09.027.
9. Mateescu MA, Ispas Szabo P, Assaad E. Chitosan and its derivatives as self-assembled systems for drug delivery. Control Drug Deliv. 2015:85-125.
10. Song P, Lu Z, Jiang Tianze, Han W, Chen X, Zhao X. Chitosan coated pH/redox-responsive hyaluronic acid micelles for enhanced tumor-targeted co-delivery of doxorubicin and siPD-L1. Int J Biol Macromol. 2022 Sep;222(A):1078-91. doi: 10.1016/j.ijbiomac.2022.09.245, PMID 36183754.
11. Jiang X, Ma M, Li M, Shao S, Yuan H, Hu F. Preparation and evaluation of novel emodin-loaded stearic acid-g-chitosan oligosaccharide nanomicelles. Nanoscale Res Lett. 2020 Apr;15(1):93. doi: 10.1186/s11671-020-03304-1, PMID 32335740.
12. Wang XH, Tian Q, Wang W, Zhang CN, Wang P, Yuan Z. *In vitro* evaluation of polymeric micelles based on hydrophobically-modified sulfated chitosan as a carrier of doxorubicin. J Mater Sci Mater Med. 2012 Apr;23(7):1663-74. doi: 10.1007/s10856-012-4627-1, PMID 22538726.
13. Tye H. Application of statistical 'design of experiments' methods in drug discovery. Drug Discov Today. 2004 Jun 1;9(11):485-91. doi: 10.1016/S1359-6446(04)03086-7, PMID 15149624.
14. Alafaghani A, Qattawi A. Investigating the effect of fused deposition modeling processing parameters using Taguchi design of experiment method. J Manuf Processes. 2018;36:164-74. doi: 10.1016/j.jmapro.2018.09.025.
15. Krishna Pm. Anchakishore babu, Palanatimamatha. Formulation and optimization of ceritinib loaded nanobubbles by box-Behnken design. Int J Appl Pharm. 2022 Jul;14(4):219-26.
16. Singh B, Kapil R, Nandi M, Ahuja N. Developing oral drug delivery systems using formulation by design: vital precepts, retrospect and prospects. Expert Opin Drug Deliv. 2011 Oct;8(10):1341-60. doi: 10.1517/17425247.2011.605120, PMID 21790511.
17. Kan S, Lu J, Liu J, Wang J, Zhao Y. A quality by design (QbD) case study on enteric-coated pellets: screening of critical variables and establishment of design space at laboratory scale. Asian J Pharm Sci. 2014 Oct;9(5):268-78. doi: 10.1016/j.ajps.2014.07.005.
18. N Politis S, Colombo P, Colombo G, M Rekkas D. Design of experiments (DoE) in pharmaceutical development. Drug Dev Ind Pharm. 2017 Jun;43(6):889-901. doi: 10.1080/03639045.2017.1291672, PMID 28166428.
19. Cheng M, Gao X, Wang Y, Chen H, He B, Xu H. Synthesis of glycyrrhetinic acid-modified chitosan 5-fluorouracil nanoparticles and its inhibition of liver cancer characteristics *in vitro* and *in vivo*. Mar Drugs. 2013 Sep;11(9):3517-36. doi: 10.3390/md11093517, PMID 24048270.
20. Lia X, Youb J, FudeCuia Y. Dub, hong Yuanb, Fuqiang Hub. Preparation and characteristics of SA grafted CS oligosaccharide polymeric micelle containing 10-hydroxycamptothecin. Asian J Pharm Sci. 2008 Feb;3(2):80-7.
21. Chen Q, Sun Y, Wang J, Yan G, Cui Z, Yin H. Preparation and characterization of glycyrrhetinic acid-modified stearic acid-grafted chitosan micelles. Artif Cells Nanomed Biotechnol. 2015;43(4):217-23. doi: 10.3109/21691401.2013.845570, PMID 24093764.
22. Patra A, Satpathy S, Shenoy AK, Bush JA, Kazi M, Hussain MD. Formulation and evaluation of mixed polymeric micelles of quercetin for treatment of breast, ovarian, and multidrug-resistant cancers. Int J Nanomedicine. 2018;13:2869-81. doi: 10.2147/IJN.S153094, PMID 29844670.
23. Xu W, Cui Y, Ling P, Li LB. Preparation and evaluation of folate-modified cationic pluronic micelles for poorly soluble anticancer drug. Drug Deliv. 2012;19(4):208-19. doi: 10.3109/10717544.2012.690005, PMID 22643055.
24. Hu FQ, Ren GF, Yuan H, Du YZ, Zeng S. Shell cross-linked stearic acid grafted chitosan oligosaccharide self-aggregated micelles for controlled release of paclitaxel. Colloids Surf B Biointerfaces. 2006 Jul;50(2):97-103. doi: 10.1016/j.colsurfb.2006.04.009, PMID 16759840.
25. Zhu QL, Zhou Y, Guan M, Zhou XF, Yang SD, Liu Y. Low-density lipoprotein-coupled N-succinyl chitosan nanoparticles co-delivering siRNA and doxorubicin for hepatocyte-targeted

therapy. Biomaterials. 2014 Jul;35(22):5965-76. doi: 10.1016/j.biomaterials.2014.03.088, PMID 24768047.

26. Salimi A, Sharif Makhmal Zadeh BSM, Kazemi M. Preparation and optimization of polymeric micelles as an oral drug delivery system for deferoxamine mesylate: *in vitro* and ex vivo studies. Res Pharm Sci. 2019 Aug;14(4):293-307. doi: 10.4103/1735-5362.263554, PMID 31516506.
27. Dash S, Murthy PN, Nath L, Chowdhury P. Kinetic modeling on drug release from controlled drug delivery systems. Acta Pol Pharm. 2010 May;67(3):217-23. PMID 20524422.
28. Kemkar K, SL, Sathiyanarayanan A, Mahadik K. 6-shogaol rich ginger oleoresin loaded mixed micelles enhances *in vitro* cytotoxicity on mcf-7 cells and *in vivo* anticancer activity against dal cells. Int J Pharm Pharm Sci. 2018 Jan;10(1):160-8. doi: 10.22159/ijpps.2018v10i1.23077.
29. An JY, Yang HS, Park NR, Koo TS, Shin B, Lee EH. Development of polymeric micelles of oleanolic acid and evaluation of their clinical efficacy. Nanoscale Res Lett. 2020;15(1):133. doi: 10.1186/s11671-020-03348-3, PMID 32572634.
30. Zhou YY, Du YZ, Wang L, Yuan H, Zhou JP, Hu FQ. Preparation and pharmacodynamics of stearic acid and poly (lactic-co-glycolic acid) grafted chitosan oligosaccharide micelles for 10-hydroxy camptothecin. Int J Pharm. 2010 Jun;393(1-2):143-51. doi: 10.1016/j.ijpharm.2010.04.025, PMID 20420886.
31. Dou J, Zhang H, Liu X, Zhang M, Zhai G. Preparation and evaluation in vitro and in vivo of docetaxel loaded mixed micelles for oral administration. Colloids Surf B Biointerfaces. 2014;114:20-7. doi: 10.1016/j.colsurfb.2013.09.010, PMID 24157590.
32. Darandale SS, Vavia PR. Cyclodextrin-based nanosponges of curcumin: formulation and physicochemical characterization. J Incl Phenom Macrocycl Chem. 2013 Apr;75(3-4):315-22. doi: 10.1007/s10847-012-0186-9.
33. Dobrovolskaia MA, Clogston JD, Neun BW, Hall JB, Anil K. Patri AK, Scott E. McNeil SE. Method for analysis of nanoparticle hemolytic properties *in vitro*. Nano Letters. 2008 Aug;8(8):2180-7. doi: 10.1021/nl0805615, PMID 18605701.
34. Song Z, Zhu W, Liu N, Yang F, Feng R. Linolenic acid-modified PEG-PCL micelles for curcumin delivery. International Journal of Pharmaceutics. 2014 Aug;471(1-2):312-21. doi: 10.1016/j.ijpharm.2014.05.059, PMID 24939613.
35. Costa P, Sousa Lobo JM. Modeling and comparison of dissolution profiles. European Journal of Pharmaceutical Sciences. 2001 May;13(2):123-133. doi: 10.1016/s0928-0987(01)00095-1, PMID 11297896.
36. Wei H, Xu L, Sun Y, Li G, Cui Z, Yan G. Preliminary pharmacokinetics of PEGpegylated oxaliplatin polylactic acid nanoparticles in rabbits and tumor-bearing mice. Artif Cells Nanomed Biotechnol. 2015 Feb;43(4):258-62. doi: 10.3109/21691401.2014.883402, PMID 24564351.
37. Termsarasab U, Cho HJ, Kim DH, Chong S, Chung SJ, Shim CK, Moon HT, Kim DD. Chitosan oligosaccharide–arachidic acid-based nanoparticles for anti-cancer drug delivery. International Journal of Pharmaceutics. 2013 Jan;441(1-2):373-80. doi: 10.1016/j.ijpharm.2012.11.018, PMID 23174411.
38. Kovacs A, Berko S, Csanyi E, Csoka I. Development of nanostructured lipid carriers containing salicyclic acid for dermal use based on the quality by design method. Eur J Pharm Sci. 2017;99:246-57. doi: 10.1016/j.ejps.2016.12.020, PMID 28012940.
39. Beg S, Saini S, Bandopadhyay S, Katare OP, Singh B. QbD-driven development and evaluation of nanostructured lipid carriers (NLCs) of olmesartan medoxomil employing multivariate statistical techniques. Drug Dev Ind Pharm. 2018 Mar;44(3):407-20. doi: 10.1080/03639045.2017.1395459, PMID 29048242.
40. Patel M, Sawant K. A quality by design concept on lipid-based nanoformulation containing antipsychotic drug: screening design and optimization using response surface methodology. J Nanomed Nanotechnol. 2017 May;08(3):1-11. doi: 10.4172/2157-7439.1000442.
41. Hu FQ, Jiang XH, Huang X, Wu XL, Yuan H, Wei XH, Yong Zhong Du. Enhanced cellular uptake of chlorine e6 mediated by stearic acid–grafted chitosan oligosaccharide micelles. Journal of Drug Targeting. 2009 Jun;17(5):384-91. doi: 10.1080/10611860902894325, PMID 19343607.
42. Du YZ, Cai LL, Li J, Zhao MD, Chen FY, Yuan H, Fu-Qiang Hu. Receptor-mediated gene delivery by folic acid-modified stearic acid-grafted chitosan micelles. International Journal of Nanomedicine. 2011;6:1559:1559-68. doi: 10.2147/IJN.S23828, PMID 21845046.
43. Nazzal S, Khan MA. Response surface methodology for the optimization of ubiquinone self-nano emulsified drug delivery system. AAPS PharmSciTech. 2002 Jan; 3(1):E3. doi: 10.1208/pt030103, PMID 12916956.
44. Wei TK, Manickam S. Response surface methodology, an effective strategy in the optimization of the generation of curcumin-loaded micelles. Asia-Pac J Chem Eng. 2012 Jan;7(Suppl 1):125-33. doi: 10.1002/apj.661.
45. Shaikh MV, Kala M, Nivsarkar M. Formulation and optimization of doxorubicin-loaded polymeric nanoparticles using Box-Behnken design: ex-vivo stability and *in vitro* activity. European Journal of Pharmaceutical Sciences. 2017;100:262-72. doi: 10.1016/j.ejps.2017.01.026, PMID 28126560.
46. Abbas G, Hanif M, Khan MA. pH-responsive alginate polymeric rafts for controlled drug release by using box behnken response surface design. Designed Monomers and Polymers. 2017 Sep;20(1):1-9. doi: 10.1080/15685551.2016.1231046, PMID 29491774.
47. Chen Q, Sun Y, Wang J, Yan G, Cui Z, Yin H, Haitian Wei. Preparation and characterization of glycyrrhetinic acid-modified stearic acid-grafted chitosan micelles. Artificial Cells Nanomedicine and Biotechnology. 2015 Oct;43(4):217-23. doi: 10.3109/21691401.2013.845570, PMID 24093764.
48. Xie YT, Du YZ, Yuan H, Hu FQ. Brain-targeting study of stearic acid–grafted chitosan micelle drug-delivery system. International Journal of Nanomedicine. 2012 Jun;7:3235-44. doi: 10.2147/IJN.S32701, PMID 22802685.
49. Mohanty AK, Mohanta GP. Dual anticancer drug-loaded methoxy poly (ethylene glycol)-poly (ε-caprolactone) block copolymeric micelles as novel drug carriers. International Journal of Pharmacy and Pharmaceutical Sciences. 2014 Sep;6(9):328-32.